Structural Safety 33 (2011) 218–231

Contents lists available at ScienceDirect

Structural Safety

journal homepage: www.elsevier.com/locate/strusafe

An asymmetric dimension-adaptive tensor-product method for reliability analysis

Chao Hu [a], Byeng D. Youn [b,*]

[a] Department of Mechanical Engineering, University of Maryland at College Park, College Park, MD 20742, USA
[b] School of Mechanical and Aerospace Engineering, Seoul National University, Seoul, Republic of Korea

ARTICLE INFO

Article history:
Received 17 February 2010
Received in revised form 4 March 2011
Accepted 4 March 2011
Available online 21 April 2011

Keywords:
Directional sparse grid
Asymmetric dimension-adaptive
Variate interaction
Reliability analysis

ABSTRACT

Reliability analysis plays an essential role in the development of structural systems. However, commonly used reliability analysis methods suffer from either the curse of dimensionality or the lack of accuracy in many structural problems. This paper presents an asymmetric dimension-adaptive tensor-product (ADATP) method to resolve the difficulties of existing reliability analysis methods. The proposed method leverages three ideas: (i) an asymmetric dimension-adaptive scheme to efficiently build the tensor-product interpolation considering both directional and dimensional importance, (ii) a hierarchical interpolation scheme using either piecewise multi-linear basis functions or cubic Lagrange splines, (iii) a hierarchical surplus as an error indicator to automatically detect the highly nonlinear regions in a random space and adaptively refine the collocation points in these regions. The proposed method has three distinct features for reliability analysis: (a) automatically detecting and adaptively reproducing tri- and higher-variate interactions, (b) greatly alleviating the curse of dimensionality, and (c) no need of response sensitivities. Several mathematical and engineering problems involving high nonlinearity are used to demonstrate the effectiveness of the ADATP method.

1. Introduction

In the past few decades, reliability analysis has been widely recognized as of great importance in the development of structural systems. Hence, various methods have been developed to assess the structural reliability while taking into account various uncertainty sources (e.g., material properties, loads, geometric tolerances). In order to formulate reliability analysis in a mathematical framework, random variables are often used to model uncertainty sources in structural systems. Reliability analysis can then be formulated as a multi-dimensional integration of a structural response function over a safety region

$$R = \int_{\Omega^S} f(\mathbf{x}) d\mathbf{x} \tag{1}$$

where R denotes the structural reliability; $f(\mathbf{x})$ denotes the joint probability density function (PDF) of the vector of random variables; $\mathbf{x} = (x^1, x^2, \ldots, x^N)^T$ models uncertainty sources such as material properties, loads, geometric tolerances; the safety domain Ω^S is defined by the limit-state function as $\Omega^S = \{\mathbf{x}: g(\mathbf{x}) < 0\}$; $g(\mathbf{x})$ is a structural performance function.

In practice, however, it is extremely difficult to perform the multi-dimensional numerical integration when the number of random variables is relatively large. The search for efficient computational procedures to estimate the reliability has resulted in a variety of numerical and simulation methods such as the first- or second-order reliability method (FORM/SORM) [1–3,11], direct or smart Monte Carlo simulation (MCS) [7–10,37], dimension reduction (DR) method [5,6,16], stochastic spectral method [4,12,14,15], and stochastic collocation method [18–31].

Among many reliability analysis methods, the first- or second-order reliability method (FORM or SORM) is most commonly used. The FORM/SORM uses the first- or second-order Taylor expansion to approximate a limit-state function at the most probable failure point (MPP) where the limit-state function separates failure and safety regions of a product (or process) response. Some major challenges of the FORM/SORM include (i) it is very expensive to build the probability density function (PDF) of the response and (ii) structural design can be expensive when employing a large number of the responses.

The direct or smart MCS provides an alternative way for multi-dimensional integration [7–10,37]. Although the direct MCS [7] produces accurate results for reliability analysis and allows for relative ease in the implementation, it demands a prohibitively large number of simulation runs. Thus, it is often used for the purpose of a benchmarking in reliability analysis. To alleviate the computational burden of the direct MCS, researchers have developed various smart MCS methods, such as the (adaptive) importance sampling methods [8–10] and the enhanced MCS method with an optimized extrapolation [37]. Despite the improved efficiency than the direct MCS, these methods are still computationally expensive.

* Corresponding author. Tel.: +82 2 880 7114; fax: +82 2 883 1315.
E-mail address: bdyoun@snu.ac.kr (B.D. Youn).

0167-4730/$ - see front matter © 2011 Elsevier Ltd. All rights reserved.
doi:10.1016/j.strusafe.2011.03.004

Nomenclature

$\mathbf{e}_k$	kth unit vector
$\mathbf{e}_k^{+/-}$	kth directional unit vector
$\mathbf{i}$	multi-index
g	performance function
l	interpolation level
M	number of collocation points
N	number of input random variables
$\mathbf{x}$	vector of input random variables
ADATP	asymmetric dimension-adaptive tensor-product
BDR	bivariate dimension reduction
DI	directional index
DR	dimension reduction
DSG	directional sparse grid
FORM	first order reliability method
MCS	Monte Carlo simulation
PCE	polynomial chaos expansion
PDF	probability density function
SORM	second-order reliability method
UDR	univariate dimension reduction

Recently, the dimension reduction (DR) method [5,6] has been proposed and is known to be a sensitivity free method for reliability analysis. This method uses an additive decomposition of a response that simplifies one multi-dimensional integration to multiple one- or two-dimensional integrations. The eigenvector dimension reduction (EDR) method [16] improves numerical efficiency and stability of the univariate dimension reduction (UDR) method with the ideas of eigenvector samples and stepwise moving least squares method with no extra expense. Results of the DR-family methods are given in the form of statistical moments. To further predict the reliability or PDF of the response, PDF generation techniques must be involved, which could increase numerical error in reliability prediction. Furthermore, performance functions with strong tri- and higher-variate interactions among random inputs require tri- and higher-variate dimension decompositions for accurate reliability analysis [6]. In such cases, the computational effort could become prohibitively large for high input dimensions, thus making the decomposition strategy infeasible.

The stochastic spectral method [4] is an emerging technique for reliability analysis of complex engineering problems. This method uses a number of response samples and generates a stochastic response surface approximation with multi-dimensional polynomials over a random space. Once the explicit response surface is constructed, MCS is often used for reliability analysis due to its convenience. The most popular stochastic spectral method is the polynomial chaos expansion (PCE) method. The original Hermite polynomial chaos basis was proposed by Wiener [14] for modeling stochastic responses with Gaussian input random variables. Xiu and Karniadakis [15] extended the method under the Askey polynomial scheme to non-Gaussian random variables (e.g., Gamma, Uniform, and Beta). For the estimation of a small failure probability, shifted and windowed Hermite polynomial chaos were proposed to enhance the accuracy of a response surface in the failure region [12]. Although the PCE method is considered to be accurate, the primary drawback of the method is the curse of dimensionality, which substantially increases the computational cost as the number of random variables increases. As demonstrated by Lee [17], the implementation of the PCE method becomes inconvenient in structural design practice since the PCE order cannot be predetermined for black-box-type problems.

The stochastic collocation (SC) method is another stochastic expansion technique that approximates a multi-dimensional random function using function values given at a set of collocation points. A comparison between the SC and PCE methods for uncertainty quantification (UQ) was discussed in [30], where the SC method was reported to consistently outperform the PCE method. In the SC method, the great improvement in reducing the curse of dimensionality in numerical integration was accomplished by Smolyak [18], who introduced the concept of the sparse grid. Since then, the sparse grid has been applied to high dimensional integration [19] and interpolation [20], UQ in reliability analysis [30] and design [31], and PDEs with deterministic inputs [21] and random inputs [22–24]. Compared to a full grid, the sparse grid achieves the same accuracy level for integration and interpolation but with a much smaller number of collocation points. Recently, the so called dimension-adaptive tensor-product (DATP) quadrature method introduced the concept of the generalized sparse grid and considered the dimensional importance indicated by an error estimator to adaptively refine the collocation points for efficient multi-dimensional integration [25]. Klimke [26] further developed this work for hierarchical interpolation by using either piecewise multi-linear basis functions or Lagrangian polynomials. In this method, all the dimensions in the random space are not considered as of equal importance and the adaptive sampling scheme automatically detects the highly nonlinear dimensions and adaptively refines the collocation points in those dimensions. In [29], a priori and a posteriori procedures are included to update a weight vector for different stochastic dimensions, which combines the advantages of conventional and dimensional-adaptive approaches. As demonstrated in [27,28], the application of the dimension-adaptive tensor-product method in stochastic problems is promising.

Compared to the conventional sparse grid interpolation, the generalized sparse grid interpolation (i.e., the dimension-adaptive tensor-product interpolation) achieves a substantially higher convergence rate by detecting important dimensions and placing more collocation points in those dimensions. In the adaptive sampling, the dimension-adaptive algorithm considers the dimensional importance while treating the positive and negative axial directions in a multi-dimensional cube as of equal importance. In many engineering applications, however, not only different dimensions but also two opposite directions (positive and negative) within one dimension often demonstrate a large difference in response nonlinearity. In such cases, it is desirable to place more collocation points in the direction with higher nonlinearity, and the dimension-adaptive algorithm may not be appropriate. To this end, this paper presents an asymmetric dimension-adaptive tensor-product (ADATP) method for structural reliability analysis. The proposed method leverages three ideas: (i) an asymmetric dimension-adaptive scheme to efficiently build the tensor-product interpolation considering both directional and dimensional importance, (ii) a hierarchical interpolation scheme using either piecewise multi-linear basis functions or cubic Lagrange splines, (iii) a hierarchical surplus as an error indicator to automatically detect the highly nonlinear regions in the random space and adaptively refine the collocation points in these regions. To facilitate the incorporation of directional importance in the adaptive interpolation scheme, the concepts of the directional sparse grid (DSG) and direction index (DI) are, for the first time, proposed. Instead of selecting the index with the largest error indicator and imposing an admissibility test on each forward index, the ADATP method precedes by selecting all the indices whose error indicators are greater than a predefined error threshold. More still, a hierarchical

interpolation scheme using cubic Lagrange splines is first proposed to eliminate numerical instability of the high-order Lagrange interpolation and maintain the smoothness property of the polynomial interpolation.

This paper is organized as follows. Section 2 reviews, under the scheme of interpolation, the stochastic collocation methods, including the conventional sparse grid method and dimensional-adaptive tensor-product method. Section 3 presents the asymmetric dimension-adaptive tensor-product method and introduces the hierarchical implementation scheme. The proposed ideas are demonstrated using several case studies in Section 4 and concluded in Section 5.

2. Review of stochastic collocation methods

Great attention has been paid to the stochastic collocation method for approximating a multi-dimensional random function due to its strong mathematical foundation and ability to achieve fast convergence for interpolation construction. This section reviews the stochastic collocation methods using the tensor-product grid, the conventional and generalized sparse grids, and the hierarchical interpolation scheme using multivariate hierarchical basis functions.

In what follows, we will model the N-dimensional real random variables $\mathbf{x} = (x^1, x^2, \ldots, x^N)^T$ in a complete probability space $(\Omega, \mathcal{A}, \mathcal{P})$, where Ω is a sample space, $\mathcal{A}$ is a σ-algebra on Ω, and $\mathcal{P}$ is a probability measure function $\mathcal{P}$: $\mathcal{A} \to [0,1]$. Then the probability density function (PDF) of the random variable x^i defines a probability mapping $f_i(x^i)$: $\Pi_i \to \mathbb{R}^+$, where the support Π_i is a one-dimensional random space of x^i. Under the assumption of statistical independence, the probabilistic characteristics of the random variables $\mathbf{x}$ can then be completely defined by the joint PDF $f(\mathbf{x}) = f_1(x^1) \cdot f_2(x^2) \cdots f_N(x^N)$ with the support $\Pi = \Pi_1 \cdot \Pi_2 \cdots \Pi_N$. If the assumption of statistical independence does not hold, that is, the random variables such as fatigue material properties (fatigue ductility coefficient and exponent) are statistically dependent, a copula [38,39] can be employed to select an appropriate dependence structure and formulate a joint CDF of the random variables based on available input data, which then allows the use of the Rosenblatt transformation [40] to transform the dependant random variables into independent standard normal random variables. A numerical investigation on how to deal with dependant random variables is provided in the subsequent case study section. Since the construction of an interpolation in the stochastic collocation method often requires a specially bounded support $\Gamma = [0,1]^N$ of the random variables $\mathbf{x}$, we first truncate any unbounded one-dimensional random space Π_i (e.g. in the case of a Gaussian random variable) to a bounded one $\Gamma_i^* = [c_i, d_i]$ that achieves a nearly full coverage of Π_i and then map any truncated one-dimensional support $[c_i, d_i]$ to [0, 1], resulting in a bounded hypercube $\Gamma = [0, 1]^N$. Let $g(\mathbf{x})$ denote a smooth, measurable performance function on $(\Omega, \mathcal{A})$, which can be treated as a one-to-one mapping between the transformed N-dimensional random space and one-dimensional space g: $[0, 1]^N \to \mathbb{R}$. In general, the performance function $g(\mathbf{x})$ cannot be analytically obtained, and the function evaluation of g for a given input $\mathbf{x}$ requires an expensive computer simulation. Therefore, it is important to employ a numerical method for reliability analysis that is capable of producing accurate probabilistic characteristics of $g(\mathbf{x})$ with an acceptably small number of function evaluations.

2.1. Classical stochastic collocation: tensor-product grid

The stochastic collocation method basically approximates the performance function g using N-dimensional interpolating functions with performance function values at a finite number of collocation points $\Theta = \{\mathbf{x}_j | \mathbf{x}_j \in \Gamma,\ j = 1, \ldots, M_T\}$. Suppose that we can obtain the performance function value $g(\mathbf{x}_j)$ at each collocation point $\mathbf{x}_j$. We then aim at building an interpolation or surrogate model of the original performance function g by using the linear combinations of these function values $g(\mathbf{x}_j)$. The sampling process to construct this interpolation can be accomplished by using the tensor-product grid, conventional sparse grid based on the Smolyak algorithm [18], or generalized sparse grid based on the dimension-adaptive tensor-product algorithm [25]. We begin by constructing the interpolation with the tensor-product grid, or the tensor-product of one-dimensional interpolation formulas.

In the one-dimensional case ($N = 1$), we can construct the following one-dimensional interpolation

$$U^i(g) = \sum_{j=1}^{m_i} a_j^i \cdot g(x_j^i) \tag{2}$$

with a set of support nodes

$$X^i = \{x_j^i | x_j^i \in [0,1], j = 1, 2, \ldots, m_i\} \tag{3}$$

where $i \in \mathbb{N}$ is the interpolation level, $a_j^i \in C([0,1])$ the jth interpolation nodal basis functions, x_j^i the jth support nodes and m_i the number of support nodes in the interpolation level i. Note that, by following the descriptions in Refs. [23,26,27], we use the superscript i to denote the interpolation level during the development of stochastic collocation methods. Two widely used nodal basis functions are piecewise multi-linear basis functions and Lagrange polynomials. Here we will briefly describe the fundamentals of piecewise multi-linear basis functions. To achieve faster error decay, the Clenshaw–Curtis grid with equidistant nodes is often used for piecewise multi-linear basis functions [26]. In the case of a univariate interpolation ($N = 1$), the support nodes are defined as

$$\begin{aligned} m_i &= \begin{cases} 1 \text{ if } i = 1 \\ 2^{i-1} + 1, \text{ if } i > 1 \end{cases} \\ x_j^i &= \begin{cases} \frac{j-1}{m_i - 1} \text{ for } j = 1, \ldots, m_i \text{ if } m_i > 1 \\ 0.5 \text{ for } j = 1, \ldots, m_i \text{ if } m_i = 1 \end{cases} \end{aligned} \tag{4}$$

The resulting set of the points fulfill the nesting property $X^i \subset X^{i+1}$ that is very useful for the hierarchical interpolation scheme detailed later. Then the univariate piecewise multi-linear basis functions, supported by the Clenshaw–Curtis grid, can be expressed as [26]

$$\begin{aligned} &a_j^i = 1 \text{ for } i = 1 \\ &a_j^i = \begin{cases} 1 - (m_i - 1) \cdot |x - x_j^i|, & \text{if } |x - x_j^i| < 1/(1 - m_i) \\ 0, & \text{otherwise} \end{cases} \end{aligned} \tag{5}$$

for $i > 1$. More detailed information on the one-dimensional interpolation can be found in [26].

Applying a sequence of formulas in Eq. (2) on the original performance function g in a nested form for all N dimensions, we can easily derive the tensor-product of multiple one-dimensional interpolation formulas as the following multi-dimensional interpolation formula

$$(U^{i_1} \otimes \cdots \otimes U^{i_N})(g) = \sum_{j_1=1}^{m_1} \cdots \sum_{j_N=1}^{m_N} (a_{j_1}^{i_1} \otimes \cdots \otimes a_{j_N}^{i_N}) \cdot g\left(x_{j_1}^{i_1}, \ldots, x_{j_N}^{i_N}\right) \tag{6}$$

where the superscript i_k, $k = 1, \ldots, N$, denotes the interpolation level along the kth dimension, U^{i_k} are the interpolation functions with the interpolation level i_k along the kth dimension and the subscript j_k, $k = 1, \ldots, N$, denotes the index of a given support node in the kth dimension. The number of function evaluations required by the tensor-product formula reads

$$M_T = m_1 \cdot m_2 \cdot \cdots \cdot m_N \tag{7}$$

Suppose that we have the same number of collocation points in each dimension, i.e., $m_1 = m_2 = \ldots = m_N \equiv m$, the total number of tensor-product collocation points is $M_T = m^N$. Even if we only have three collocation points ($m = 3$) in each dimension, this number ($M_T = 3^N$) still grows very quickly as the number of dimensions is increased (e.g., $M_T = 3^{10} \approx 6 \times 10^4$, for $N = 10$). Thus, we need more efficient sampling schemes than the tensor-product grid to reduce the amount of computational effort for the multi-dimensional interpolation. The search for such sampling schemes has resulted in sparse grid methods of which the fundamentals will be briefly introduced in subsequent sections.

2.2. Smolyak algorithm: conventional sparse grid

Compared to the classical tensor-product algorithm, the Smolyak algorithm achieves an order of magnitude reduction in the number of collocation points while maintaining the approximation quality of the interpolation by imposing an inequality constraint on the summation of multi-dimensional indices [18]. This inequality leads to special linear combinations of tensor-product formulas such that the interpolation error remains the same as for the tensor-product algorithm.

The Smolyak formulas $A(q, N)$ are special linear combinations of tensor-product formulas. Using tensor-products of one-dimensional interpolation functions, the Smolyak algorithm constructs a sparse multi-dimensional interpolation, expressed as [20]

$$A_{q,N}(g) = \sum_{q-N+1 \leqslant |\mathbf{i}| \leqslant q} (-1)^{q-|\mathbf{i}|} \cdot \binom{N-1}{q-|\mathbf{i}|} \cdot (U^{i_1} \otimes \cdots \otimes U^{i_N})(g) \tag{8}$$

where $\mathbf{i} = (i_1, \ldots, i_N)$ is the multi-index, and $|\mathbf{i}| = i_1 + \ldots + i_N$. The above formula indicates that the Smolyak algorithm builds the multi-dimensional interpolation by considering one-dimensional functions of interpolation levels $i_1, \ldots, i_N$ under the constraint that the sum of these interpolation levels lies within the range $[q - N + 1, q]$. With the incremental interpolant, $\Delta^i = U^i - U^{i-1}$, $U^0 = 0$, the Smolyak formulas can be equivalently written as [20]

$$\begin{aligned} A_{q,N}(g) &= \sum_{|\mathbf{i}| \leqslant q} (\Delta^{i_1} \otimes \cdots \otimes \Delta^{i_N})(g) \\ &= A_{q-1,N}(g) + \sum_{|\mathbf{i}| = q} (\Delta^{i_1} \otimes \cdots \otimes \Delta^{i_N})(g) \end{aligned} \tag{9}$$

The above formulas suggest that the Smolyak algorithm improves the interpolation by utilizing all the previous interpolation formulas $A_{q-1,N}$ and the current incremental interpolant with the order q. If we select the sets of support nodes in a nested fashion (i.e., $X^i \subset X^{i+1}$) to obtain recurring points (e.g., the Clenshaw–Curtis grid) when extending the interpolation level from i to $i + 1$, we only need to compute function values at the differential grids that are unique to X^{i+1}, $X_\Delta^{i+1} = X^{i+1}/X^i$. In such cases, to build a sparse multi-dimensional interpolation with the order q, we only need to compute function values at the nested sparse grid

$$\begin{aligned} H_{q,N} &= \bigcup_{|\mathbf{i}| \leqslant q} (X_\Delta^{i_1} \times \cdots \times X_\Delta^{i_N}) = H_{q-1,N} \cup \Delta H_{q,N} \\ \Delta H_{q,N} &= \bigcup_{|\mathbf{i}| = q} (X_\Delta^{i_1} \times \cdots \times X_\Delta^{i_N}) \end{aligned} \tag{10}$$

where $\Delta H_{q,N}$ denotes the grid points required to increase an interpolation order from $q - 1$ to q.

Although the Smolyak algorithm greatly reduces the number of collocation points for the multi-dimensional interpolation compared to the tensor-product algorithms, there is still possibility of further reducing the number of function evaluations in cases where the performance function exhibits different degrees of nonlinearity in the stochastic dimensions. To achieve such a reduction, one must adaptively detect the dimensions with higher degrees of nonlinearity and assign more collocation points to those dimensions. This can be accomplished by using the dimension-adaptive tensor-product algorithm, which is detailed in the next subsection.

2.3. Dimension-adaptive tensor-product algorithm: generalized sparse grid

For a given interpolation level l, the conventional sparse grid requires the index set $\mathbf{I}_{l,N} = \{\mathbf{i} \; | |\mathbf{i}| \leqslant l + N\}$ to build the interpolation $A(l + N, N)$. If we loosen the admissibility condition on the index set, we can construct the index set of the generalized sparse grid [25]. An index set $\mathbf{I}$ is called admissible if for all $\mathbf{i} \in \mathbf{I}$,

$$\mathbf{i} - \mathbf{e}_k \in \mathbf{I} \text{ for } 1 \leqslant k \leqslant N, i_k > 1 \tag{11}$$

Here, $\mathbf{e}_k$ is the kth unit vector. This admissibility condition still satisfies the telescopic property of the incremental interpolant $\Delta^i = U^i - U^{i-1}$. Thus, we can take advantage of the previous interpolation to construct a better interpolation by just sampling the differential grids that are unique to the finer interpolation, as shown in Eqs. (9) and (10). In each step of the algorithm, an error indicator is assigned to each multi-index $\mathbf{i}$. The multi-index $\mathbf{i}_t$ with the largest estimated error is selected for an adaptive refinement, since possibly a larger error reduction can achieved. The admissible indices in the forward neighborhood of $\mathbf{i}_t$ are added to the index set $\mathbf{I}$. The forward neighborhood of an index $\mathbf{i}$ can be defined as

$$\mathbf{I}_F(\mathbf{i}) = \{\mathbf{i} + \mathbf{e}_k, \quad 1 \leqslant k \leqslant N\} \tag{12}$$

In each step, the newly added indices are called active indices and grouped as an active index set $\mathbf{I}_A$, whereas those indices whose forward neighborhood have been refined are called old indices and grouped as an old index set $\mathbf{I}_O$. The overall index set $\mathbf{I}$ comprises of the active and old index sets: $\mathbf{I} = \mathbf{I}_A \cup \mathbf{I}_O$. For more details of the dimension-adaptive algorithm, readers are referred to References [25] and [26].

It is noted that, in the dimension-adaptive algorithm, the generalized sparse grid construction allows for an adaptive detection of the important dimensions and thus a more efficient refinement compared to the conventional sparse grid interpolation [24,25]. However, in engineering practice, not only different dimensions but also two opposite directions (positive and negative) within one dimension often demonstrate a large difference in response nonlinearity. In such cases, it is desirable to place more points in the direction with higher nonlinearity, and the dimension-adaptive algorithm may not be appropriate for this purpose.

2.4. Hierarchical interpolation scheme using multivariate hierarchical basis functions

For the dimension-adaptive interpolation, the hierarchical interpolation scheme provides a more convenient way for error estimation than the nodal interpolation scheme [26]. Here, we start with the derivation of hierarchical interpolation formulae in the case of the univariate interpolation, which takes advantage of the nested characteristic of grid points (i.e., $X^i \subset X^{i+1}$). Recall the incremental interpolant in Section 2.2, $\Delta^i = U^i - U^{i-1}$. Based on Eq. (2) and $U^{i-1}(g) = U^i(U^{i-1}(g))$, we can write [26]

$$\begin{aligned} \Delta^i(g) &= U^i(g) - U^i(U^{i-1}(g)) \\ &= \sum_{x_j^i \in X^i} a_j^i \cdot g(x_j^i) - \sum_{x_j^i \in X^i} a_j^i \cdot U^{i-1}(g)(x_j^i) \\ &= \sum_{x_j^i \in X^i} a_j^i \cdot (g(x_j^i) - U^{i-1}(g)(x_j^i)) \end{aligned} \tag{13}$$

Since for all $x_j^i \in X^{i-1}$, $g(x_j^i) - U^{i-1}(g)(x_j^i) = 0$, and Eq. (13) can be rewritten as

$$\Delta^i(g) = \sum_{x_j^i \in X_\Delta^i} a_j^i \cdot (g(x_j^i) - U^{i-1}(g)(x_j^i)) \tag{14}$$

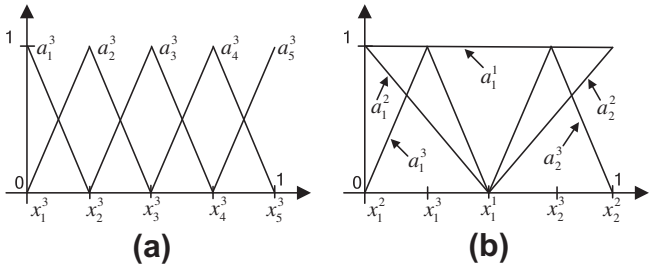

Fig. 1. Nodal basis functions $a_j^3, x_j^3 \in X^3$ (a) and hierarchical basis functions a_j^i with the support nodes $x_j^i \in X_\Delta^i, i = 1,2,3$ (b) for the Clenshaw–Curtis grid.

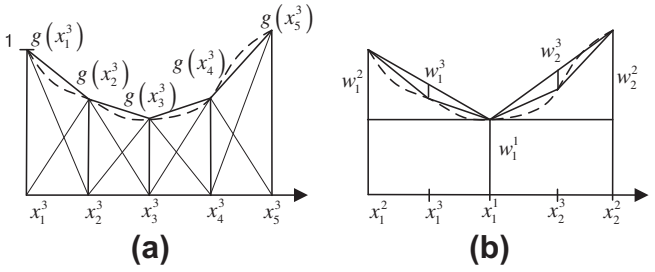

Fig. 2. Nodal (a) and hierarchical (b) interpolations in 1D.

Since $X^i \subset X^{i+1}$, the number of grid points in X_Δ^i reads

$$m_\Delta^i = m^i - m^{i-1} \tag{15}$$

By denoting the jth element of X_Δ^i by x_j^i, Eq. (14) can be rewritten as

$$\Delta^i(g) = \sum_{j=1}^{m_\Delta^i} a_j^i \cdot \underbrace{(g(x_j^i) - U^{i-1}(g)(x_j^i))}_{w_j^i} \tag{16}$$

Here, w_j^i is defined as the hierarchical surplus, which indicates the interpolation error of a previous interpolation at the node x_j^i of the current interpolation level i. The bigger the hierarchical surpluses, the larger the interpolation errors. For smooth performance functions, the hierarchical surpluses approach zero as the interpolation level goes to infinity. Therefore, the hierarchical surplus can be used as a natural candidate for error estimation and control [26]. Fig. 1 shows the comparison between the hierarchical and nodal basis functions with piecewise linear spline and Clenshaw–Curtis grid [26]. Fig. 2 illustrates the comparison between the hierarchical and nodal interpolation. Based on the Smolyak formula in Eq. (9), a multivariate hierarchical interpolation formula can be obtained as [26]

$$\begin{aligned} A_{q,N}(g) &= A_{q-1,N}(g) + \Delta A_{q,N}(g) \\ &= A_{q-1,N}(g) + \sum_{|\mathbf{i}|=q} \sum_{\mathbf{j}} \\ &\quad \times \underbrace{(a_{j_1}^{i_1} \otimes \cdots \otimes a_{j_N}^{i_N})}_{a_{\mathbf{j}}^{\mathbf{i}}} \cdot \underbrace{(g(x_{j_1}^{i_1}, \cdots, x_{j_N}^{i_N}) - A_{q-1,N}(g)(x_{j_1}^{i_1}, \cdots, x_{j_N}^{i_N}))}_{w_{\mathbf{j}}^{\mathbf{i}}} \end{aligned} \tag{17}$$

3. Asymmetric dimension-adaptive tensor-product method

As an attempt to enhance the adaptive feature of the dimension-adaptive algorithm, we, for the first time, introduce the concept of the directional sparse grid (DSG) which allows for the considerations of both directional and dimensional importance. Furthermore, a hierarchical interpolation scheme using cubic Lagrange splines is proposed for eliminating numerical inaccuracy of the high-order Lagrange interpolation as well as maintaining the smoothness property of the polynomial interpolation. The hierarchical ADATP interpolation and UQ and reliability analysis using the proposed ADATP method will also be presented in subsequent sections.

3.1. Directional sparse grid (DSG)

For the construction of the directional sparse grid (DSG), a conventional index i in the case of the univariate interpolation is decomposed into positive and negative directional index (DI) sets as

$$\mathbf{I}^{\mathrm{D}} = \{i^+, i^-\} \tag{18}$$

where the positive DI i^+ corresponds to the DSG which belong to the index i and whose values are greater than the value (0.5) of the center grid point, and the negative DI i^- corresponds to the DSG which belong to the index i and whose values are smaller than 0.5. For the multivariate case ($N > 1$), we obtain a tensor-product formula of DI sets for a multi-index $\mathbf{i}$ as

$$\mathbf{I}^{\mathrm{D}} = \mathbf{I}_1^{\mathrm{D}} \times \cdots \times \mathbf{I}_N^{\mathrm{D}} \tag{19}$$

where $\mathbf{I}_k^D = \{i_k^+, i_k^-\}$, $1 \leqslant k \leqslant N$. Here, the forward neighborhood of a multi-dimensional DI $\mathbf{i}^d \in \mathbf{I}^D$ is defined as the N indices $\{\mathbf{i}^{\mathrm{d}} + \mathbf{e}_k^{+/-}\}$, $1 \leqslant k \leqslant N$, and the sign of kth directional unit vector $\mathbf{e}_k^{+/-}$ is the same with that of the kth index element i_k^d (i_k^+ or i_k^-) of $\mathbf{i}^{\mathrm{d}}$. If i_k^d is equal to 1, i.e., the corresponding collocation point is located at 0.5, both the positive and negative directional unit vectors are employed to obtain the forward neighborhood in that dimension. Fig. 3 shows the conventional multi-index and the proposed DI for a 2D interpolation with the same set of the collocation points. From this

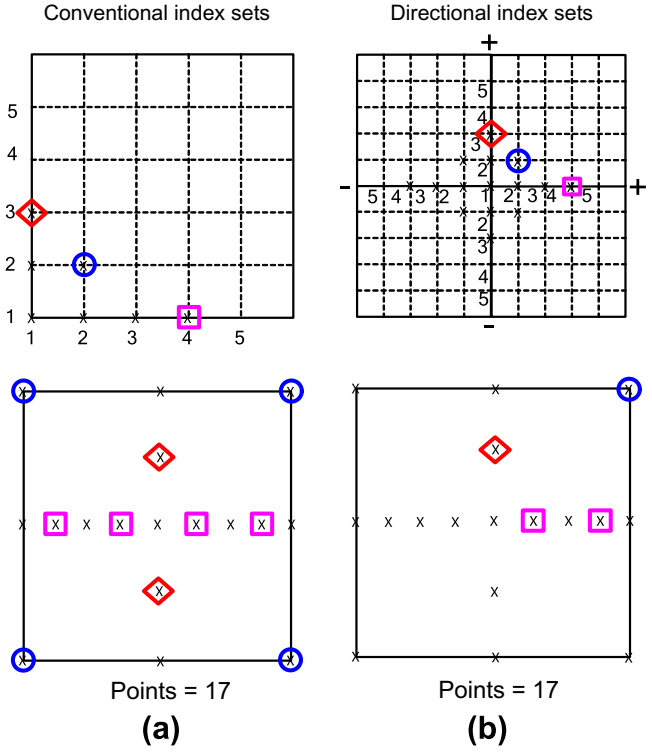

Fig. 3. Conventional (a) and directional (b) index sets in 2D. Top row: index sets including (1, 3) and (1^+, 3^+) denoted by ◇, (2, 2) and (2^+, 2^+) denoted by O, (4, 1) and (4^+, 1^+) denoted by □. Bottom row: corresponding collocation points.

figure, it is observed that the proposed DI divides the conventional index space into the four quadrants. In subsequent sections, it will be seen that this division allows for an adaptive refinement of the collocation points in these quadrants. In general, it is noted that the DI divides the conventional multi-index space into 2^N N-hyperoctants for more precise refinement.

3.2. Hierarchical interpolation scheme using cubic Lagrange splines

For the dimension-adaptive interpolation, the hierarchical interpolation scheme provides a more convenient way for the error estimation than the nodal interpolation scheme. In the case of singularities or discontinuities in the random space, the piecewise multi-linear basis function provides a strong local support for the adaptive algorithm. The detailed information regarding the selection of grid type and numerical scheme can be found in [26]. The Clenshaw–Curtis grid with equidistant nodes is recommended for piecewise multi-linear basis functions and is thus utilized in the ADATP method. In the case of a smooth function, the polynomial interpolation provides a faster error decay with increasing numbers of grid points than the piecewise multi-linear interpolation. However, the high-order Lagrange interpolation may give an inaccurate estimation of the performance function between collocation points due to severe oscillation, especially when the grid points are asymmetrically distributed with respect to the center point. To avoid this numerical inaccuracy and take advantage of the polynomial interpolation, a hierarchical interpolation scheme using cubic Lagrange splines is proposed for the ADATP method.

3.3. Choice of sparse grid type

For the Lagrange interpolation, it is known that the Chebyshev–Gauss–Lobatto grid is a good choice due to its Chebyshev-based node distribution and its nesting characteristic [26]. However, this type of grid may not be appropriate for local adaptivity without a global support provided by Lagrange polynomials. In contrast, the Clenshaw–Curtis grid with equidistant nodes is more suitable for a local support provided by the cubic Lagrange spline function. In addition, it possesses the nesting characteristic. Thus, we propose to use the Clenshaw–Curtis grid as collocation points. In the case of a univariate interpolation ($N = 1$), the support nodes are defined in Eq. (4). As mentioned earlier, the resulting set of the points fulfill the nesting property $X^i \subset X^{i+1}$, and therefore $H_{q-1,N} \subset H_{q,N}$.

3.4. Univariate nodal basis functions

The interpolation for smooth functions can be improved by replacing piecewise multi-linear basis functions by cubic Lagrange splines. The univariate nodal basis functions for cubic Lagrange splines can be expressed as [32]

$$a_j^i = 1 \text{ for } i = 1$$

$$a_j^i = \begin{cases} \prod_{\substack{l=j-1 \\ l\neq j}}^{j+2} \frac{x-x_l^i}{x_j^i-x_l^i} & \text{if } x \in [x_j^i, x_{j+1}^i], \quad j = 2,\ldots,m_i-2 \\ \prod_{l=j+1}^{j+2} \frac{x-x_l^i}{x_j^i-x_l^i} & \text{if } x \in [x_j^i, x_{j+1}^i], \quad j = 1 \\ \prod_{\substack{l=j-1 \\ l\neq j}}^{j+1} \frac{x-x_l^i}{x_j^i-x_l^i} & \text{if } x \in [x_j^i, x_{j+1}^i], \quad j = m_i-1 \\ 0 & \text{otherwise} \end{cases} \tag{20}$$

for $i > 1$. In Eq. (20), the function value at endpoint x_j^i, $j = 1$, m_i, is not given. Then the polynomial on the interval $[x_2^i, x_3^i]$ is extended to the interval $[x_1^i, x_2^i]$ and the polynomial on the interval $[x_{mi-2}^i, x_{mi-1}^i]$ to the interval $[x_{mi-1}^i, x_{mi}^i]$. We observed that these extensions caused negligible sacrifice of the interpolation accuracy on the intervals $[x_1^i, x_2^i]$ and $[x_{mi-1}^i, x_{mi}^i]$.

3.5. Asymmetric dimension-adaptive tensor-product (ADATP) interpolation

Based on the proposed concepts of the DI and DSG, the overall procedure of the ADATP interpolation is briefly summarized in Table 1. The relative error indicator used in the interpolation scheme can be defined for a DI $\mathbf{i}$ (see Fig. 3b) as

$$\varepsilon_r(\mathbf{i}) = \frac{1}{(g_{\max} - g_{\min})M_{\mathbf{i}}} \sum_{\mathbf{j}} |w_{\mathbf{j}}^{\mathbf{i}}| \tag{21}$$

where $w_{\mathbf{j}}^{\mathbf{i}}$ are the hierarchical surpluses of the collocation points $\mathbf{X}^i = X_\Delta^{i_1} \times \cdots \times X_\Delta^{i_N}$, with $\mathbf{j} = (j_1,\ldots,j_N)$, $j_k = 1,\ldots,m_\Delta^{i_k}$, $1 \leqslant k \leqslant N$, and $M_{\mathbf{i}} = m_\Delta^{i_1} \cdot m_\Delta^{i_2} \cdot \cdots \cdot m_\Delta^{i_N}$. It is noted that, for simplicity, we use $\mathbf{i} = (i_1,\ldots,i_N)$ instead of $\mathbf{i}^{\mathrm{d}} = (i_1^d,\ldots,i_N^d)$ to denote a multi-dimensional DI and that the term "index" in the description of the ADATP method refers to the DI. The pseudo code for the ADATP algorithm is given in the Appendix A. Under the proposed scheme of asymmetric sampling, we expect that the error decay be at least as fast as that of the dimension-adaptive tensor-product interpolation.

3.6. Uncertainty quantification (UQ) and reliability analysis

Once the asymmetric dimension-adaptive sampling procedure is completed, an approximate function $\hat{g}$ of the original performance function g can be obtained by interpolation using hierarchical basis functions at collocation points. Thus, any probabilistic characteristics of $g(\mathbf{x})$, including statistical moments, reliability, and PDF, can be easily estimated by performing MCS. For example, any rth moment can be calculated as

$$\beta_r \cong \int \hat{g}^r(\mathbf{x}) f(\mathbf{x}) d\mathbf{x} = E(\hat{g}^r(\mathbf{x})) = \lim_{ns\to\infty} \frac{1}{ns} \sum_{j=1}^{ns} \hat{g}^r(\mathbf{x}_j) \tag{22}$$

where β_r is the rth moment of the performance function $g(\mathbf{x})$; $f(\mathbf{x})$ is the joint PDFs; $\mathbf{x}_j$ is the jth realization of $\mathbf{x}$; and ns is the sampling size. For reliability estimation, let us define an approximate safe domain for the performance function g as

$$\hat{\Omega}^S = \{\mathbf{x} : \hat{g}(\mathbf{x}) < 0\} \tag{23}$$

Therefore, the reliability R can also be estimated by performing MCS as

$$R \cong \int I_{\hat{\Omega}^S}(\mathbf{x}) f(\mathbf{x}) d\mathbf{x} = E(I_{\hat{\Omega}^S}(\mathbf{x})) = \lim_{ns\to\infty} \frac{1}{ns} \sum_{j=1}^{ns} I_{\hat{\Omega}^S}(\mathbf{x}_j) \tag{24}$$

Table 1
Procedure of the proposed ADATP interpolation.

STEP 1	Set an initial interpolation level l $(q - N) = 0$; set the initial old index set $\mathbf{I}_{\mathrm{O}} = \emptyset$ and the initial active index set $\mathbf{I}_{\mathrm{A}} = \{\mathbf{i}\}$, where the initial active DI $\mathbf{i} = (1,\ldots,1)$ is the center point $(0.5,\ldots,0.5)$; set an initial relative error indicator $\varepsilon_r(\mathbf{i}) = 1$
STEP 2	Select a trial index set $\mathbf{I}_{\mathrm{T}}$ (from $\mathbf{I}_{\mathrm{A}}$) with the error indicator greater than a relative error threshold value ε_{C}; move the active index set $\mathbf{I}_{\mathrm{A}}$ to the old index set $\mathbf{I}_{\mathrm{O}}$. If $\mathbf{I}_{\mathrm{T}} = \emptyset$, go to STEP 7
STEP 3	Select and remove the trial index $\mathbf{i}_{\mathrm{t}}$ with the largest error indicator from $\mathbf{I}_{\mathrm{T}}$; if none, go to STEP 6. If the number of the collocation points M exceeds the maximum number $M_{\max}$, go to STEP 7
STEP 4	Generate the forward neighborhood $\mathbf{I}_{\mathrm{F}}$ of $\mathbf{i}_{\mathrm{t}}$ and add $\mathbf{I}_{\mathrm{F}}$ to the active index set $\mathbf{I}_{\mathrm{A}}$
STEP 5	Compute the hierarchical surplus of each new added point based on the collocation points in the old index set and compute the error indicator of each active index. Go to STEP 3.
STEP 6	Set an interpolation level $l = l + 1$ and go to STEP 2
STEP 7	Construct an explicit interpolation $\hat{g}$ of the performance function g

where $I[\cdot]$ is an indicator function of safe or fail state such that

$$I_{\hat{\Omega}^S}(\mathbf{x}_j) = \begin{cases} 1, & \mathbf{x}_j \in \hat{\Omega}^S \\ 0, & \mathbf{x}_j \in \Omega \setminus \hat{\Omega}^S \end{cases} \tag{25}$$

It should be noted that the MCS performed here employs the explicit interpolation $\hat{g}$ instead of the original performance function g and is thus inexpensive. We also note that the way of approximating the response function over the entire (truncated) input domain allows for the derivation of any probabilistic characteristics (e.g., statistical moments, reliability, and PDF) based on the same set of collocation points and can be used for design problems that require both moment estimation and reliability analysis such as reliability-based robust design optimization [43–45].

3.7. Remarks

Several important remarks regarding the properties of the ADATP method are listed as follows.

3.7.1. Remark 1 – potential benefits

In the proposed method, the DI divides the conventional multi-index space into 2^N N-hyperoctants, thus enabling asymmetric refinements among these hyperoctants. Therefore, for a performance function with unequal degrees of nonlinearity in 2^N N-hyperoctants, the ADATP method is expected to outperform the DATP method in terms of efficiency.

3.7.2. Remark 2 – determination of an interpolation domain

It is noted that when the random space Π is unbounded, e.g. in the case of Gaussian random variables, we need to truncate it to a bounded one Γ that achieves a nearly full coverage of the original random space Π. Without loss of generality, we consider the case of N-dimensional independent standard Gaussian random vector $\mathbf{x}$, the probability that a realization of the original random space Π belongs to the truncated random space $\Gamma^* = [-\lambda, \lambda]^N$ can be expressed as

$$\begin{aligned} P(\Gamma^*|\Pi) &= \int I_{\Gamma^*}(\mathbf{x}) f(\mathbf{x}) d\mathbf{x} = \lim_{ns\to\infty} \frac{1}{ns} \sum_{j=1}^{ns} I_{\Gamma^*}(\mathbf{x}_j) \\ &= [\Phi(\lambda) - \Phi(-\lambda)]^N \end{aligned} \tag{26}$$

In the current study, we used $\lambda = 3.5$, which, for example, gives $P(\Gamma^*|\Pi) = 0.9954$ for $N = 10$. We note that the truncation has a negative effect on the accuracy of reliability analysis, especially for problems with small numbers of random variables (i.e., small N in Eq. (26)) and low probabilities of failure, and that the truncated interpolation domain for a specific problem should be carefully determined based on the understanding of this problem. More conservative criteria may guarantee higher accuracy but creates a larger interpolation domain that requires more computational effort. Since the goal in this work is to develop an asymmetric interpolation scheme for uncertainty qualification and reliability analysis, this paper does not address the issues regarding how a choice of the interpolation domain affects numerical accuracy and efficiency of reliability analysis and how to achieve an optimum λ for a given problem.

3.7.3. Remark 3 – discretion on an error threshold

We also note that the relative error threshold ε_C greatly affects the convergence rate and accuracy of the asymmetric dimension-adaptive sampling. A larger ε_C leads to faster error decay but results in a lower level of interpolation accuracy. A zero threshold, as an extreme case, results in a conventional sparse grid construction. In the current study, we used $\varepsilon_C = 0.10$ for most engineering cases. Under the hierarchical interpolation scheme, ε_C allows a user to put a preference between the convergence rate and accuracy.

4. Case studies

Six mathematical and engineering examples are given in this section to demonstrate the effectiveness of the ADATP method. The first two mathematical examples dealt with the response surfaces with asymmetric nonlinearity, which were designed to compare the performances of the ADATP and DATP methods for interpolation. The third mathematical example and subsequent three engineering examples were used for studying the computational accuracy and efficiency of the proposed method for UQ and reliability analysis.

4.1. Mathematical example I: response surface with line singularity

Consider a mathematical function

$$g(\mathbf{x}) = \frac{1}{|0.25 - x_1^2 - x_2^2| + 0.1} \tag{27}$$

where the two random variables were assumed to be statistically independent and uniformly distributed between 0 and 1. It is noted that, for notational convenience, we use the notation x_k instead of x^k to denote the kth random variable for $k = 1, \ldots, N$ in this section. This modified function from [21] shows a line singularity in the third quadrant of the square $\Omega = [0,1]^2$. We further defined the interpolation error ε_I as

$$\varepsilon_I = \max_{j=1,\ldots,ns} |g(\mathbf{x}_j) - \hat{g}(\mathbf{x}_j)| \tag{28}$$

where ns denotes the number of Monte Carlo samples for interpolation and was set to 1,000,000 in this example. A relative error threshold $\varepsilon_C = 0.10$ was used in the ADATP method. Fig. 4 illustrates the error decay and PDF approximations of the DATP and ADATP methods, both of which, for comparison purpose, employed the piecewise multi-linear basis functions e as the hierarchical basis functions and the Clenshaw–Curtis grid as the grid type. It should be noted that, since the ADATP and DATP methods employ different schemes for generating new collocation points, the numbers of collocation points achieved by both methods could be different. However, a meaningful comparison can still be carried out by observing a general trend of error decay. In Fig. 4a, the ADATP method shows faster error decay and more accurate PDF approximation, compared to that of the DATP method. This is because the ADATP method identified high nonlinearity in the third quadrant and adaptively added collocation points to the quadrant region (see the shaded region in Fig. 5a) while the DATP method treated all quadrants as of equal importance and thus assigns points equally to all quadrants (see Fig. 5b). This example verifies that, for a performance function with unequal degrees of nonlinearity in 2^N N-hyperoctants, the ADATP method is more efficient than the DATP method.

4.2. Mathematical example II: smooth response surface

Consider a mathematical function

$$g(\mathbf{x}) = \frac{\sinh(\pi(1 - x_1)) \sin(\pi x_2)}{\sinh(\pi)} \tag{29}$$

where the two random variables were assumed to be statistically independent and uniformly distributed between 0 and 1. This smooth function from [21] demonstrates higher nonlinearity in the second and third quadrants of the square $[0,1]^2$. A relative error

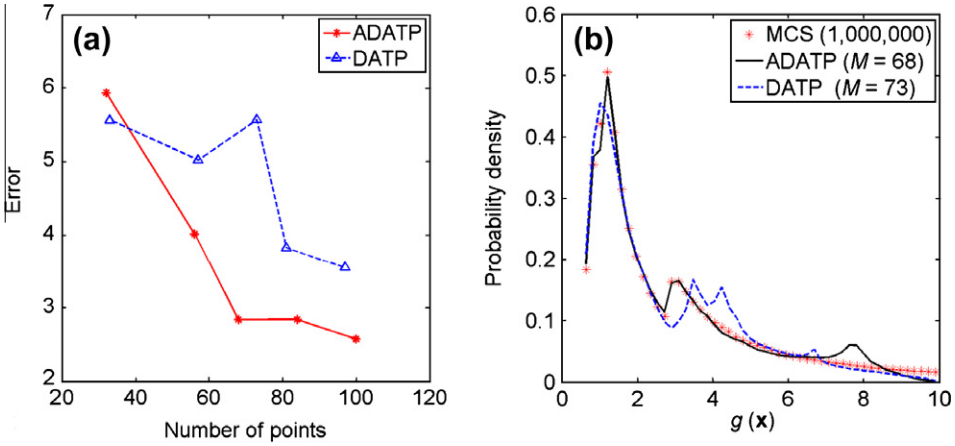

Fig. 4. Error decay (a) and PDF approximations (b) of the DATP and ADATP methods for example I.

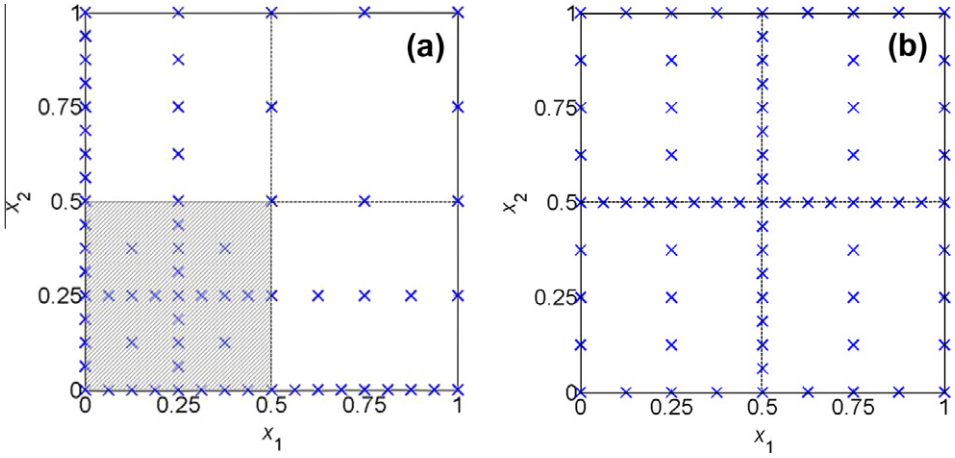

Fig. 5. Collocation points of the ADATP method ($M = 68$) (a) and the DATP method ($M = 73$) (b) for example I.

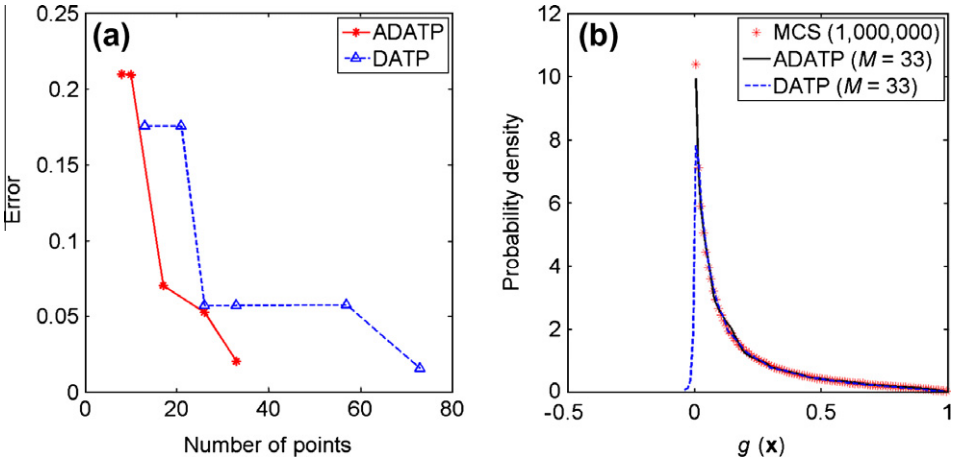

Fig. 6. Error decay (a) and PDF approximation (b) of the DATP and ADATP methods for example II.

threshold $\varepsilon_C = 0.10$ was used in the ADATP method. Fig. 6 illustrates the error decay and PDF approximation of the DATP and ADATP methods, both of which employed the piecewise multi-linear basis functions as the hierarchical basis functions and the Clenshaw–Curtis grid as the grid type. The ADATP method required only 33 points to achieve the error level around 0.0203, while the DATP method required 73 points to achieve approximately the same error level. Besides, the ADATP method gives more accurate PDF approximation, especially around the left bound. This is due to the fact that the ADATP method identified high nonlinearity in

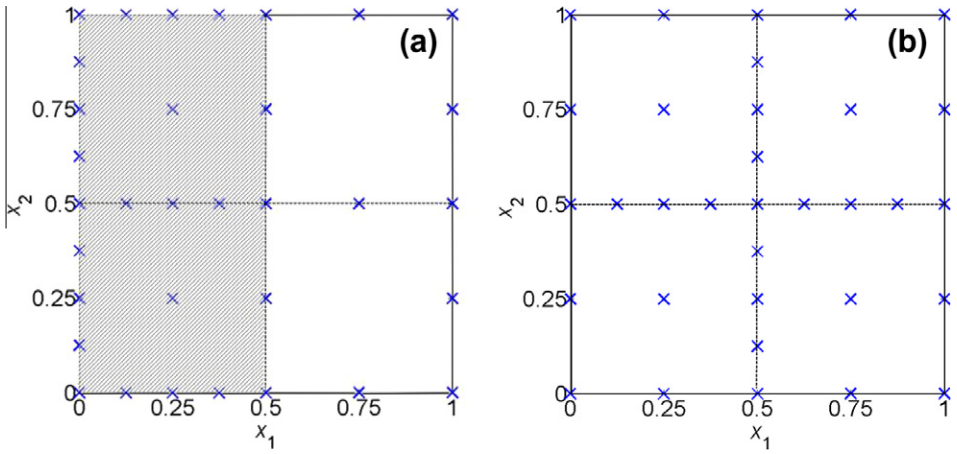

Fig. 7. Collocation points of the DATP method ($M = 33$) (a) and the ADATP method ($M = 33$) (b) for example II.

the second and third quadrants and adaptively added collocation points to the quadrant regions (see the shaded regions in Fig. 7a), while the DATP method treated all quadrants as of equal importance and thus assigns points equally to all quadrants (see Fig. 7b). Thus, this example further verifies that, for problems with unequal degrees of nonlinearity in 2^N N-hyperoctants, the ADATP method is more efficient than the DATP method.

4.3. Mathematical example III: trivariate interaction

Consider a mathematical function

$$g(\mathbf{x}) = \sum_{k=1}^{N=5} (x_k - 1)^2 - \sum_{k=3}^{N=5} x_k^r x_{k-1}^r x_{k-2}^r \tag{30}$$

Table 2
Moment estimations by the ADATP and dimension reduction methods ($L = 1.0$).

r	Mean (μ_g)				Standard deviation (σ_g)			
	UDR[a]	BDR[a]	ADATP[a]	MCS[b]	UDR	BDR	ADATP	MCS
0	0.2946	0.3283	0.3246	0.3336	0.1436	0.2119	0.2738	0.2691
1	4.7588	5.4681	5.3999	5.5650	2.9811	4.4782	5.7853	5.5953
2	5.6486	6.3037	6.2180	6.4028	2.9942	4.4296	5.6848	5.5264
3	5.8516	6.4914	6.4154	6.5855	2.9131	4.3343	5.6112	5.4657

[a] UDR and BDR required 21 and 181 function evaluations (FEs), respectively; ADATP required 121 FEs.
[b] MCS required 1,000,000 FEs at MC sample points.

where the five random variables were assumed to be statistically independent and uniformly distributed between 0 and L. The proposed ADATP method with $\varepsilon_C = 0.10$, $M_{\max} = 120$ and cubic Lagrange splines as the hierarchical basis functions was employed to compute the mean μ_G and standard deviation σ_g of $g(\mathbf{x})$. These two moments were calculated using the UDR and BDR integrations [6] based on a fully tensorized Gauss–Legendre quadrature technique [33] with the number of one-dimensional quadrature points $m_l = 5$. Two cases were considered: (i) Case 1: increasing the trivariate order ($r = 0$, 1, 2, or 3; $L = 1.0$); (ii) Case 2: increasing the uncertainty of input random variables (L increases from 0.1 to 1.0; $r = 2$). The results for Case 1 were summarized in Table 2. Both the BDR and ADATP methods provide good approximations of the mean μ_g, when compared with the results of MCS for a trivariate order up to 3. However, the UDR method can not accurately estimate μ_g for any trivariate order. Regarding the standard deviation σ_g, the ADATP method gives a consistently more accurate estimate, while both the UDR and BDR methods fail to give sufficiently accurate estimates. The results of σ_g for Case 2 are plotted in Fig. 8. All three methods can give a good approximation when the uncertainty (controlled by L) of input random variables is small. However, as the uncertainty increases, the ADATP method becomes superior to the UDR and BDR methods. This comparison with the UDR and BDR methods suggests that the ADATP method is better in terms of both accuracy and efficiency when the trivariate interaction is strong as in this problem. The ADATP method outperforms the UDR and BDR methods because of the following two reasons: (i) the UDR and BDR methods do not consider trivariate

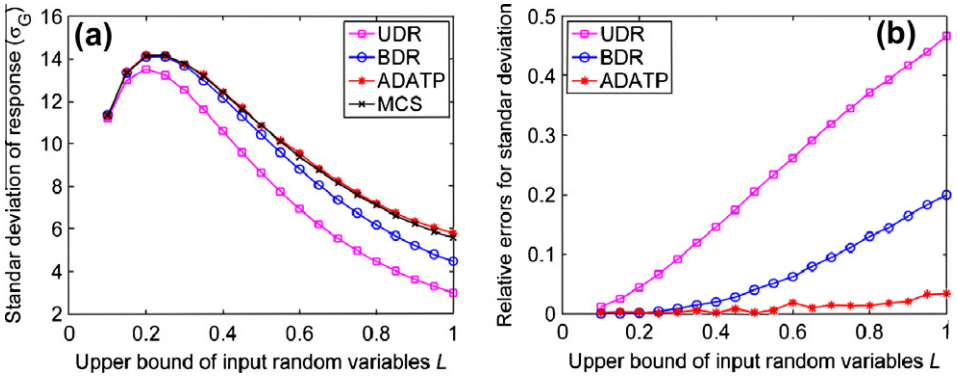

Fig. 8. Estimates (a) and relative errors (b) of standard deviations for increasing values of L.

interactions; (ii) without an adaptive sampling scheme, the UDR and BDR methods may unnecessarily assign many uni- or bivariate sample points in regions with small nonlinearity. Even if we could resolve the first limitation by increasing S in the S-variate dimension reduction (DR) technique, the second limitation still remains unresolved. In fact, it is often difficult or impractical to predetermine S in the S-variate DR technique. In contrast, the ADATP method is capable of automatically detecting tri- and higher-variate interactions and generating corresponding collocation points to reproduce the interactions in the interpolation. Therefore, the ADATP method is distinctively advantageous from the S-variate dimension reduction (DR) technique.

4.4. Fortini's clutch: very low and high reliability levels

This example is the Fortini's clutch, as shown in Fig. 9. This problem has been extensively used in the field of tolerance design [34,35]. As shown in Fig. 9, the overrunning clutch is assembled by inserting a hub and four rollers into the cage. The contact angle, y, between the vertical line and the line connecting the centers of two rollers and the hub, is expressed in terms of the random component variables, x_1, x_2, x_3, and x_4 as follows:

$$y(\mathbf{x}) = \arccos\left(\frac{x_1 + 0.5(x_2 + x_3)}{x_4 - 0.5(x_2 + x_3)}\right) \tag{31}$$

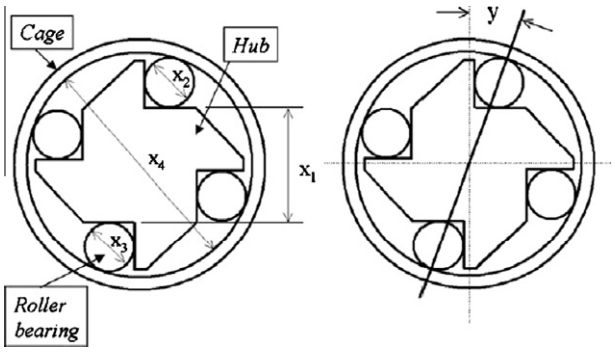

Fig. 9. Fortini's clutch.

Table 3
Input random variables for the Fortini's clutch example.

Component	Distri. type	Mean (mm)	Std. dev. (mm)	Parameters for non-normal distributions
x_1	Beta	55.29	0.0793	$\alpha_1 = \beta_1 = 5.0$[a]
x_2	Normal	22.86	0.0043	–
x_3	Normal	22.86	0.0043	–
x_4	Rayleigh	101.60	0.0793	$\sigma_4 = 0.1211$[b]

[a] $55.0269 \leqslant x_1 \leqslant 55.5531$.
[b] $x_4 \geqslant 55.5531$.

The statistical information of the random variables is summarized in Table 3. The limit-state function was defined as $(y - c)$ where c specifies a limit-state value. In the ADATP method, $\varepsilon_C = 0.10$, $M_{\max} = 50$, and cubic Lagrange splines were employed as the hierarchical basis functions. Two cases were tested, one with the assumption of statistical independence between the random variables to compare the accuracy and efficiency of various reliability analysis methods, and the other with a statistical dependence modeled by a copula to demonstrate how the ADATP method deals with dependant random variables.

4.4.1. Case I: statistical independence

In this case, we assume the four random variables to be mutually independent. Table 4 summarizes the uncertainty analysis results of the ADATP method with comparison to MCS, the UDR method (with the Pearson PDF generation system), and FORM. To reflect the variation in the probability estimate by MCS, we computed the error bounds with a 95% confidence level. The error bound with a $100(1-\alpha)\%$ confidence can be computed as [42]

$$\varepsilon_S = z_{1-\alpha/2}\sqrt{\frac{P(1-P)}{N_S}} \tag{32}$$

where $z_{1-\alpha/2}$ is the $100(1-\alpha/2)$th percentile of the standard normal distribution, P is the probability estimate by MCS and NS is the number of MCS samples. For a 95% confidence level, $\alpha = 0.05$ and $z_{1-\alpha/2} = 1.96$. As can be seen from Table 4, the ADATP method produced more accurate reliability estimates than the other methods at various reliability levels, including two very low levels (i.e., around 10^{-3}) and a very high level (i.e., around $1–10^{-3}$). The errors of the UDR method in reliability estimations come from moment estimations and PDF approximations with the Pearson system, while the errors of FORM are due to the increased response nonlinearity by the transformation between the original random x-space and the standard normal random u-space.

4.4.2. Case II: statistical dependence

In this case, the random variables x_1 and x_4 were assumed to have a statistical dependence, or more specifically, a nonlinear correlation described by a copula. In what follows, we intend to demonstrate how the ADATP method resolves the nonlinear correlation.

Table 4
Uncertainty analysis results for the Fortini's clutch example (Case I).

	ADATP	MCS	$4N+1$ UDR	FORM
Mean (rad)	0.1219	0.1219	0.1219	–
Std. dev. (rad)	0.0116	0.0117	0.0116	–
Skewness	−0.0770	−0.0511	0.0952	–
Kurtosis	2.8322	2.8805	2.8775	–
$\Pr(y < 4°)$	0.000000	0.000000 (±0.000000[a])	0.000018	0.000082
$\Pr(y < 5°)$	0.001133	0.001228 (±0.000069[a])	0.000486	0.002375
$\Pr(y < 6°)$	0.071830	0.073825 (±0.000513[a])	0.066697	0.087707
$\Pr(y < 7°)$	0.502174	0.502903 (±0.000980[a])	0.514469	0.520360
$\Pr(y < 8°)$	0.939208	0.936671 (±0.000477[a])	0.933024	0.934922
$\Pr(y < 9°)$	0.999639	0.999233 (±0.000054[a])	0.998696	0.999112
$\Pr(4° < y < 9°)$	0.999639	0.999233 (±0.000054[a])	0.998678	0.999030
No. FE	39	1000,000	17	(100/100/25/10/15/25)[b]

[a] Error bounds computed with a 95% confidence level.
[b] 100 function evaluations for $\Pr(y < 4°)$ and $\Pr(y < 5°)$, 25 for $\Pr(y < 6°)$, 10 for $\Pr(y < 7°)$, 15 for $\Pr(y < 8°)$, 25 for $\Pr(y < 9°)$.

4.4.2.1. Introduction of copula. In statistics, a copula is defined by Roser [38] as "a function that joins or couples multivariate joint distribution functions to their one-dimensional marginal distribution functions", or "multivariate distribution functions whose one-dimensional margins are uniform on the interval [0,1]".

Let F be an N-dimensional cumulative distribution function (CDF) with continuous marginal CDFs $F_1, F_2, \ldots, F_N$. Then according to Sklar's theorem, there exists a unique N-copula C such that

$$F(x_1, x_2, \ldots, x_N) = C(F_1(x_1), F_2(x_2), \ldots, F_N(x_N)) \tag{33}$$

It then becomes clear that a copula formulates a joint CDF with the support of separate marginal CDFs and a dependence structure. The copula is capable of constructing the joint CDF in real applications with different types of marginal CDFs or dependence structures. Various general types of dependence structures can be represented, corresponding to various copula families, such as Gaussian, Clayton, Frank, and Gumbel. Let $u_i = F_i(x_i)$, $i = 1, 2$, and then we can formulate a bivariate Clayton copula as

$$C(u_1, u_2|\alpha) = (u_1^{-\alpha} + u_2^{-\alpha} - 1)^{-1/\alpha} \tag{34}$$

More detailed information on copula families can be found in References [38,39].

4.4.2.2. Rosenblatt transformation. The Rosenblatt transformation has been used extensively for mapping the correlated random variables onto the independent standard normal variables [40]. The successive conditioning procedures for a vector of correlated random variables are defined as

$$\begin{aligned} z_1 &= \varphi^{-1}[F_1(x_1)] \\ z_2 &= \varphi^{-1}[F_2(x_2|x_1)] \\ &\vdots \\ z_N &= \varphi^{-1}[F_N(x_N|x_1, x_2, \cdots, x_{N-1})] \end{aligned} \tag{35}$$

where $z_1, z_2, \ldots, z_N$ denote the independent standard random variables after the transformation, $\varphi^{-1}(\cdot)$ denotes the inverse CDF of a standard normal variable, $F_i(x_i|x_1, x_2, \ldots, x_{i-1})$ denotes the CDF of x_i conditioned on $X_1 = x_1$, $X_2 = x_2$, $\ldots$, $X_{i-1} = x_{i-1}$, and can be expressed as

$$F_i(x_i|x_1, x_2, \cdots, x_{i-1}) = \frac{\int_{-\infty}^{x_i} f_i(x_1, x_2, \cdots, x_{i-1}, \tau)d\tau}{f_{i-1}(x_1, x_2, \cdots, x_{i-1})} \tag{36}$$

where $f_i(x_1, x_2, \ldots, x_i)$ denotes the marginal joint PDF of $x_1, x_2, \ldots, x_i$. In particular, the Rosenblatt transformation for a bivariate copula is given as [41]

$$\begin{aligned} z_1 &= \varphi^{-1}[u_1] = \varphi^{-1}[F_1(x_1)] \\ z_2 &= \varphi^{-1}[C(u_2|u_1)] = \varphi^{-1}[C(F_2(x_2)|F_1(x_1))] \end{aligned} \tag{37}$$

where

$$\begin{aligned} C(u_2|u_1) &= P(U_2 \leqslant u_2|U_1 = u_1) \\ &= \lim_{\Delta u_1 \to 0} \frac{C(u_1 + \Delta u_1, u_2) - C(u_1, u_2)}{\Delta u_1} = \frac{\partial C(u_1, u_2)}{\partial u_1} \end{aligned} \tag{38}$$

After the Rosenblatt transformation, the independent standard normal variables are used as the Gaussian input variables for the ADATP method.

4.4.2.3. Results and discussion. The rank correlation coefficient was used to quantify the nonlinear correlation. We assumed the rank

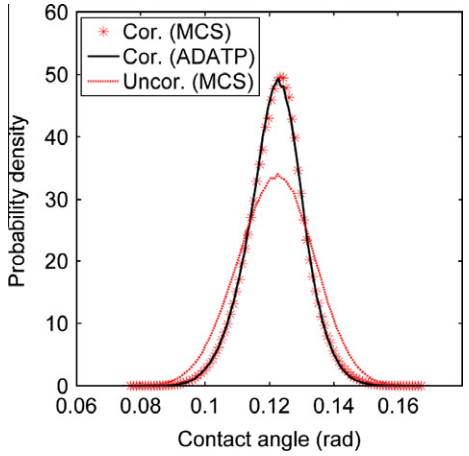

Fig. 10. PDF approximations for the Fortini's clutch example.

Table 5
Uncertainty analysis results for the Fortini's clutch example (Case II).

	ADATP	MCS
Mean (rad)	0.1221	0.1222
Std. dev. (rad)	0.0084	0.0085
Skewness	−0.0607	−0.0981
Kurtosis	3.3509	3.5953
Pr($y < 4.5°$)	0.000000	0.000000 (±0.000000[a])
Pr($y < 5.5°$)	0.001850	0.002486 (±0.000098[a])
Pr($y < 6.5°$)	0.144443	0.142989 (±0.000686[a])
Pr($y < 7.5°$)	0.861061	0.867337 (±0.000665[a])
Pr($y < 8.5°$)	0.998335	0.997820 (±0.000091[a])
Pr($4.5° < y < 8.5°$)	0.998335	0.997820 (±0.000091[a])
No. FE	45	1000,000

[a] Error bounds computed with a 95% confidence level.

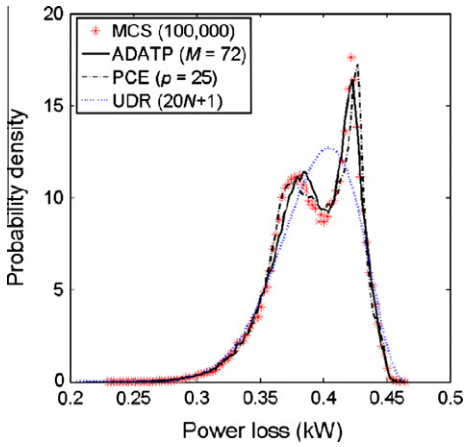

Fig. 11. PDF approximations for the V6 engine example.

Table 6
Uncertainty analysis results for the V6 engine example.

	ADATP	MCS	PCE ($p = 25$)	$20N + 1$ UDR	FORM
Mean (kW)	0.3935	0.3935	0.3934	0.3935	–
Std. dev. (kW)	0.0311	0.0310	0.0311	0.0314	–
Skewness	−0.6062	−0.5883	−0.5742	−0.5393	–
Kurtosis	3.0567	3.0828	3.0566	3.0974	–
Pr(PL < 0.3)	0.0055	0.0054 (±0.0005[a])	0.0057	0.0048	0.0057
No. FE	72	100,000	625	41	15

[a] Error bounds computed with a 95% confidence level.

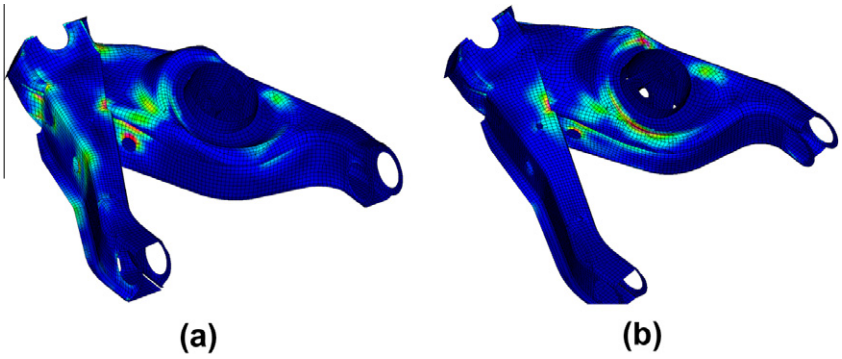

Fig. 12. Stress contours for load case 2 (a) and load case 8 (b).

correlation coefficient Kendall's τ to be 0.35 and the corresponding copula parameter to be 1.08. The Rosenblatt transformation detailed in the previous section was employed to transform the dependant input variables x_1 and x_4 into independent standard normal variables. To illustrate the effect of statistical nonlinear correlation on the system response, we plotted the PDFs for both correlated and uncorrelated cases in Fig. 10. It shows that the effect of the nonlinear correlation on the response PDF is significant and that the ADATP method accurately reproduces the peak and tail regions of the PDF. Quantitative results of uncertainty analysis are summarized in Table 5, where we can observe satisfactory results produced by the ADATP method.

4.5. V6 gasoline engine power loss: bimodal PDF

This example is the V6 gasoline engine problem used by Lee [17]. The performance function considered in this example is the power loss due to the friction between the piston ring and the cylinder liner, oil consumption, blow-by, and liner wear rate. A ring/liner subassembly simulation model was used to compute the power loss. The simulation model has four input parameters, the ring surface roughness x_1, liner surface roughness x_2, linear Young's modulus x_3 and linear hardness x_4. Of the total four inputs, the first two, ring surface roughness x_1 and linear surface roughness x_2, were treated as random inputs following normal distributions with mean 4.0 and 6.119 μm, respectively, and with unit variance. The other two inputs, linear Young's modulus x_3 and linear hardness x_4, were treated as deterministic inputs fixed at 80 GPa and 240 BHV, respectively. It has been shown in [17] that the power loss has a bimodal PDF. To predict the bimodal shape of the PDF, the ADATP method used $\varepsilon_C = 0.005$, $M_{\max} = 70$, and cubic Lagrange splines as the hierarchical basis functions. Fig. 11 shows the PDF approximations by the 25th order PCE with a fully tensorized Gauss–Hermite quadrature ($m_I = 25$), the UDR method, the ADATP method and MCS. Both the ADATP and PCE methods provide reasonably accurate approximations of the irregularly shaped PDF. The UDR method fails to represent the irregular shape of this PDF mainly due to the following two reasons: (i) errors in moment estimations propagate to errors in the PDF construction; and (ii) the first four moments are not sufficient to accurately construct the PDF. The uncertainty analysis results in Table 6 suggest that the number of function evaluations of the ADATP method is much smaller than that of the PCE method with a fully tensorized Gaussian quadrature. In this example, the FORM requires the smallest number of function evaluations while still producing a good reliability estimate. The small error produced by the FORM is due to the nonlinearity of the power loss function. However, the usage of FORM cannot be used for cases that require the construction of a complete PDF and subsequent uncertainty propagations.

4.6. Lower control A-arm: nonlinear fatigue reliability

Vehicle suspension systems experience intense loading conditions throughout their service lives. Control-arms act as the backbone of the suspension system, through which the majority of these loads are transmitted [36]. Therefore, it is crucial that the fatigue life of control-arms be high enough to fulfill the design requirement. A HMMWV lower control-arm was used for fatigue reliability analysis using the ADATP method.

The lower control-arm was modeled with plane stress elements using 54,666 nodes, 53,589 elements, and 327,961 DOFs, where all welds were modeled using rigid beam elements. Hyper-Works 8.0 was used for finite element modeling and design parameterization. ANSYS 10.0 was used for stress analyses for 14 load cases at four joints for the A-arm: a ball joint, a spring-damper joint and front and rear pivot bushing joints, respectively. The stress contours for two loading cases are shown in Fig. 12. The fe-safe 5.0 was employed for durability analysis based on the dynamic stress results from ANSYS. A preliminary durability analysis was executed in fe-safe to estimate the fatigue life of the HMMWV A-Arm and to predict the critical regions that experience a low fatigue life. For this preliminary durability analysis, the fatigue life for crack initiation was calculated using the equivalent von Mises stress-life approach at all surface nodes of the mechanical component (i.e., A-arm) in order to predict the critical regions. More accurate durability analysis was then carried using the strain-life method at the selected critical regions of the A-arm that experience short life spans.

The random variables are the thicknesses of the eight major components of the control-arm, as shown in Fig. 13. The statistical

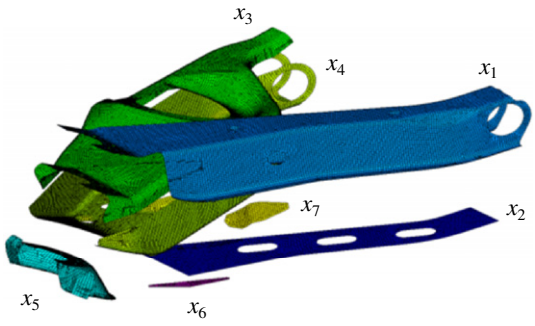

Fig. 13. Seven thickness variables (x_8 not shown).

Table 7
Input random variables for the lower control A-arm example.

Component	Distri. type	Mean (in)	Std. dev. (in)
x_1	Normal	0.157	0.006
x_2	Normal	0.183	0.006
x_3	Normal	0.178	0.009
x_4	Normal	0.200	0.007
x_5	Normal	0.312	0.013
x_6	Normal	0.250	0.009
x_7	Normal	0.200	0.007
x_8	Normal	0.201	0.009

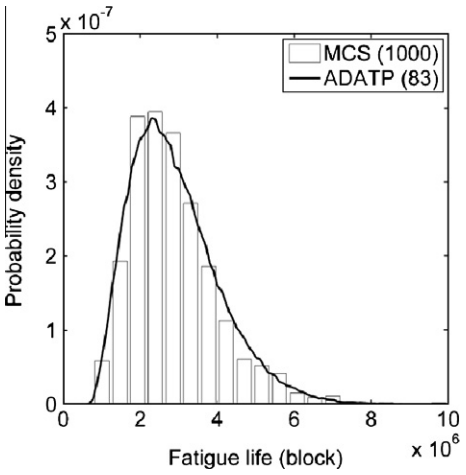

Fig. 14. PDF approximations for the lower control A-arm example.

Table 8
Uncertainty analysis results for the lower control A-arm example.

	ADATP	MCS
Mean (blocks)	2.9014E+6	2.8866E+6
Std. dev. (blocks)	1.1501E+6	1.1612E+6
Skewness	8.9795E−1	1.2608E+0
Kurtosis	4.0504E+0	5.8083E+0
$R = \Pr(L > 2.0 \times 10^6)$	0.768	0.774 (±0.026[a])
$R = \Pr(L > 1.5 \times 10^6)$	0.920	0.930 (±0.016[a])
$R = \Pr(L > 1.0 \times 10^6)$	0.992	0.993 (±0.005[a])
No. FE	83	1000

[a] Error bounds computed with a 95% confidence level.

information of these random variables is summarized in Table 7. From a worst-case scenario analysis, one hotspot with the smallest fatigue life was found at the rear pivot bushing joint and was selected for fatigue reliability analysis. In this case study, the fatigue reliability is defined as $R = \Pr(L > L^t)$, where L^t denotes the target fatigue life.

The ADATP method with $\varepsilon_C = 0.10$, $M_{\max} = 80$ and cubic Lagrange splines was used to evaluate the fatigue reliability at the selected hotspot. The ADATP method allows for a stochastic response surface approximation from a small number of deterministic finite element and fatigue analyses, through constructing an explicit hierarchical interpolation formula with respect to the random inputs. Conducting the MCS on the explicit interpolation formula gives the full probability information (i.e., moments, reliability and PDF) of the fatigue life. A direct MCS with 1000 samples was carried out as a reference. Fig. 14 shows the PDF approximations by the ADATP method and MCS, where we can observe a good agreement between the two methods. Table 8 summarizes the uncertainty analysis results, where the ADATP method outperforms MCS in terms of efficiency while still maintaining good accuracy for moderate (between 0.70 and 0.80), high (between 0.90 and 0.95) and very high reliability levels (above 0.99). The 95% confidence intervals of the MCS reliability estimates include the corresponding ADATP estimates for all three reliability levels.

5. Conclusion

The asymmetric dimension-adaptive tensor-product (ADATP) method is proposed for efficient reliability analysis involving high nonlinearity. The ADATP method possesses three technical contributions: (i) an asymmetric dimension-adaptive sampling scheme considering both directional and dimensional importance, (ii) the concepts of the directional sparse grid (DSG) and directional index (DI) for the systematic generation of asymmetric collocation points, (iii) a hierarchical interpolation scheme using cubic Lagrange splines for eliminating the numerical inaccuracy of the high-order Lagrange interpolation.

It was found that the asymmetric dimension-adaptive sampling scheme and the hierarchical interpolation method showed better accuracy and efficiency than the DATP method in the case of unequal degrees of nonlinearity in 2^N N-hyperoctants. The better performance can be attributed to the fact that the ADATP method identifies the highly nonlinear hyperoctants and assigns more collocation points to these regions, while the DATP treats all the hyperoctants as of equal importance and thus assigns points equally.

A limited comparative study between the ADATP method and the widely used reliability analysis methods, including FORM and moment-based reliability (mostly DR) methods, was also conducted in this work. Our initial results suggest that the ADATP method achieves higher accuracy and comparable efficiency for problems with moderate dimensions. The higher accuracy can be attributed to the automatic detection and adaptive reproduction of significant variate interactions in structural system responses, including tri- and higher-variate interactions. We also expect that the ADATP method perform well for high dimensional engineering problems as exemplified in the lower control A-arm example discussed in this work. Relative to the DR and PCE methods, the ADATP method has the advantage of the complexity reduction in the algorithm controls, since the desired interpolation accuracy and resource constraints allow a user to easily define a relative error threshold and maximum number of collocation points. In contrast, it is often difficult or impractical to predetermine S in the S-variate DR technique, or the expansion order and the number of one-dimensional quadrature points in the PCE method. Furthermore, the proposed ADATP method can approximate a multimodal PDF. Future research will investigate the effect of a relative error threshold on the convergence rate as well as integrate the proposed method with system reliability analysis and design optimization.

Acknowledgments

The authors would like to acknowledge that this research is partially supported by US National Science Foundation (NSF) under Grant No. GOALI-0729424, U.S. Army TARDEC by the STAS contract (TCN-05122), by General Motors under Grant No. TCS02723, and by the SNU-IAMD.

Appendix A

This appendix presents the pseudo code of the proposed ADATP algorithm as follows:

Pseudo code:	Symbols:	
$\mathbf{i} = (1, \ldots, 1)$	$\mathbf{I}_O$	old index set
$\mathbf{I}_O = \varnothing$, $\mathbf{I}_A = \{\mathbf{i}\}$	$\mathbf{I}_A$	active index set
$l = 0$, $\varepsilon_r = 1$, $M = 1$	$\mathbf{I}_T$	trial index set
while $(\max_{I_A}(\boldsymbol{\varepsilon}_r) > \varepsilon_c \&\& M < M_{\max})$	$\mathbf{I}_F(\mathbf{i}_t)$	forward neighborhood of trial index
select $\mathbf{I}_T \subset \mathbf{I}_A$ with $\boldsymbol{\varepsilon}_r(\mathbf{I}_T) > \varepsilon_c$	ε_r	relative error indicator
$\mathbf{I}_O = \mathbf{I}_O \cup \mathbf{I}_A$, $\mathbf{I}_A = \varnothing$	ε_c	relative error threshold
while $(\mathbf{I}_T \neq \varnothing \&\& M < M_{\max})$	$g_{\max}$	maximum function value
select $\mathbf{i}_t \subset \mathbf{I}_T$ with $\varepsilon_r(\mathbf{i}_t) > \varepsilon_r(\mathbf{i}_r), \forall \mathbf{i}_r \in \mathbf{I}_T$	$g_{\min}$	minimum function value
$\mathbf{I}_F(\mathbf{i}_t) = \{\mathbf{i}_t + e_k^{+/-}, \quad 1 \leqslant k \leqslant N\}$	$e_k^{+/-}$	kth directional unit vector
$\mathbf{I}_A = \mathbf{I}_A \cup \mathbf{I}_F(\mathbf{i}_t)$	adatpstep	step hierarchical interpolation function
$\mathbf{w}^{\mathbf{i}_f} = g(\mathbf{X}^{\mathbf{i}_f}) - \text{adatpstep}(\mathbf{I}_O, \{\mathbf{w}^{\mathbf{I}_O}\}, \{\mathbf{X}^{\mathbf{i}_f}\})$		
$M = M + M_{\mathbf{i}_f}$		
$\varepsilon_r(\mathbf{i}_f) = \frac{1}{(g_{\max} - g_{\min}) M_{\mathbf{i}_f}} \sum_{\mathbf{j}} \lvert w_{\mathbf{j}}^{\mathbf{i}_f} \rvert$		
endwhile		
$l = l + 1$		
endwhile		

References

[1] Hasofer AM, Lind NC. Exact and invariant second-moment code format. ASCE J Eng Mech 1974;100(1):111–21.
[2] Breitung K. Asymptotic approximations for multinormal integrals. ASCE J Eng Mech 1984;110(3):357–66.
[3] Tvedt L. Two second-order approximations to the failure probability. Section on structural reliability. A/S Vertas Research, Hovik, Norway; 1984.
[4] Ghanem RG, Spanos PD. Stochastic finite elements: a spectral approach. New York: Springer; 1991.
[5] Rahman S, Xu H. A univariate dimension-reduction method for multi-dimensional integration in stochastic mechanics. Probab Eng Mech 2004;19(4):393–408.
[6] Xu H, Rahman S. A generalized dimension-reduction method for multi-dimensional integration in stochastic mechanics. Int J Numer Meth Eng 2004;61(12):1992–2019.
[7] Rubinstein RY. Simulation and the Monte Carlo method. New York: Wiley; 1981.
[8] Fu G, Moses F. Importance sampling in structural system reliability. In: Proceedings of ASCE joint specialty conference on probabilistic methods, Blacksburg, VA; 1988. p. 340–3.
[9] Au SK, Beck JL. A new adaptive importance sampling scheme for reliability calculations. Struct Saf 1999;21(2):135–58.
[10] Hurtado JE. Filtered importance sampling with support vector margin: a powerful method for structural reliability analysis. Struct Saf 2007;29(1):2–15.
[11] Youn BD, Choi KK. An investigation of nonlinearity of reliability-based design optimization approaches. J Mech Des 2004;126(3):403–11.
[12] Paffrath M, Wever U. Adapted polynomial chaos expansion for failure detection. J Comput Phys 2007;226(1):263–81.
[14] Wiener N. The homogeneous chaos. Am J Math 1938;60(4):897–936.
[15] Xiu D, Karniadakis GE. The Wiener–Askey polynomial chaos for stochastic differential equations. SIAM J Scient Comput 2002;24(2):619–44.
[16] Youn BD, Zhimin X, Wang P. Eigenvector dimension reduction (EDR) method for sensitivity-free uncertainty quantification. Struct Multidiscipl Optim 2008;37(1):13–28.
[17] Lee SH, Chen W. A comparative study of uncertainty propagation methods for black-box-type problems. Struct Multidiscipl Optim 2009;37(3):239–53.
[18] Smolyak S. Quadrature and interpolation formulas for tensor product of certain classes of functions. Soviet Math – Doklady 1963;4:240–43.
[19] Gerstner T, Griebel M. Numerical integration using sparse grids. Numer Algorithms 1998;18(3–4):209–32.
[20] Barthelmann V, Novak E, Ritter K. High dimensional polynomial interpolation on sparse grids. Adv Comput Math 2000;12(4):273–88.
[21] Griebel M. Adaptive sparse grid multilevel methods for elliptic PDEs based on finite differences. Computing 1998;61(2):151–79.
[22] Xiu D, Hesthaven JS. High order collocation methods for the differential equation with random inputs. SIAM J Scient Comput 2005;27(3):1118–39.
[23] Xiu D. Efficient collocational approach for parametric uncertainty analysis. Commun Comput Phys 2007;2(2):293–309.
[24] Nobile F, Tempone R, Webster C. A sparse grid collocation method for elliptic partial differential equations with random input data. SIAM J Numer Anal 2008;46(5):2309–45.
[25] Grestner T, Griebel M. Dimension-adaptive tensor-product quadrature. Computing 2003;71(1):65–87.
[26] Klimke A. Uncertainty modeling using fuzzy arithmetic and sparse grids. PhD thesis, Universität Stuttgart, Shaker Verlag, Aachen; 2006.
[27] Ganapathysubramanian B, Zabaras N. Sparse grid collocation schemes for stochastic natural convection problems. J Comput Phys 2007;225(1):652–85.
[28] Ma X, Zabaras N. An adaptive hierarchical sparse grid collocation algorithm for the solution of stochastic differential equations. J Comput Phys 2009;228(8):3084–113.
[29] Nobile F, Tempone R, Webster C. An anisotropic sparse grid stochastic collocation method for partial differential equations with random input data. SIAM J Numer Anal 2008;46(5):2411–42.
[30] Eldred MS, Burkardt J. Comparison of non-intrusive polynomial chaos and stochastic collocation methods for uncertainty quantification. In: Proceedings of the 47th AIAA aerospace sciences meeting, Orlando, FL; 2009.
[31] Eldred MS, Webster CG, Constantine P. Design under uncertainty employing stochastic expansion methods. In: Proceedings of the 12th AIAA/ISSMO multidisciplinary analysis and optimization conference, Victoria, British Columbia, Canada; 2008.
[32] Kvasov BI. Methods of shape-preserving spline approximation. Singapore: World Scientific Publ. Co. Inc.; 2000.
[33] Abramowitz M, Stegun, IA. Handbook of mathematical functions. 9th ed. New York: Dover Publications, Inc.; 1972.
[34] Creveling CM. Tolerance design: a handbook for developing optimal specification. Reading, MA: Addison-Wesley; 1997.
[35] Wu CC, Chen Z, Tang GR. Component tolerance design for minimum quality loss and manufacturing cost. Comput Ind 1998;35(3):223–32.
[36] Youn BD, Zhimin X, Wang P. Reliability-based robust design optimization using the eigenvector dimension reduction (EDR) method. Struct Multidiscipl Optim 2007;37(5):475–92.
[37] Naess A, Leira BJ, Batsevych O. System reliability analysis by enhanced Monte Carlo simulation. Struct Saf 2009;31(5):349–55.
[38] Roser BN. An introduction to copulas. New York: Springer; 1999.
[39] Noh Y, Choi KK, Du L. Selection of copula to generate input joint CDF for RBDO. In: Proceedings of ASME international design engineering technical conferences (IDETC) and computers and information in engineering conference (CIE), IDETC2008-49494, Brooklyn, New York, United States; 2008.
[40] Rosenblatt M. Remarks on a multivariate transformation. Ann Math Statist 1952;23:470–2.
[41] Hu C, Youn BD. Adaptive-sparse polynomial chaos expansion for reliability analysis and design of complex engineering systems. Struct Multidiscipl Optim 2011;43(3):419–42.
[42] Law AM, Kelton WD. Simulation modeling and analysis. New York: McGraw-Hill; 1982.
[43] Youn BD, Choi KK, Yi K. Reliability-based robust design optimization using the performance moment integration method and case study of engine gasket-sealing problem. In: Proceedings of SAE 2005 world congress, Detroit, MI, United States; 2005.
[44] Youn BD, Choi KK, Yi K. Performance moment integration (PMI) method for quality assessment in reliability-based robust design optimization. Mech Based Des Struct Machines 2005;33:185–213.
[45] Lee SH, Chen W, Kwak BM. Robust design with arbitrary distributions using Gauss-type quadrature formula. Struct Multidiscipl Optim 2009;39(3):227–43.